Numerical Methods in Civil Engineering, 7-3 (2023) 13-25

Numerical Methods in Civil Engineering

Journal Homepage: https://nmce.kntu.ac.ir/

Numerical Study of Seismic Performance of Reinforced Concrete Moment-Resisting Frame with Cold-Joint

Ehsan Karimi* and Vahid Reza Kalatjari**

ARTICLE INFO

RESEARCH PAPER

Article history:
Received:
January 2022.
Revised:
June 2022.
Accepted:
July 2022.

Keywords:
Cold-joint,
Fracture mechanics,
Pushover analysis,
Seismic performance,
Ductility

Abstract:

In this paper, the seismic performance of reinforced concrete moment-resisting frame with cold-joint subjected to monotonic lateral load has been studied numerically using Pushover analysis. Two modes of fracture may occur for cold-joint in a frame subjected to in-plane loading. The modes are Mode-I (stress orthogonal to the local plane of the crack surface) and Mode-II (stress parallel to the crack surface but orthogonal to the crack front). In order to model cold-joint and verify its behavior in mode I and mode II fracture mechanics, first the three-point bending beam with an initial notch in the middle of the span and then the S-shaped specimen, used in the push-off test, have been modeled and validated. Furthermore, a single-story single-span bare frame has been monotonically modeled at first and validated by laboratory results. Subsequently, cold-joint has been added to this frame and analyzed. Moreover, to investigate the effect of the number of spans, the considered frame has been analyzed with two and three spans in both monolithic (MJ) and the cold-joint (CJ) statuses. In order to investigate the seismic performance, parameters such as ultimate lateral capacity, stiffness, and ductility have been evaluated. The results of this study show that in general, the presence of cold-joint in the frame has little effect on the ultimate lateral capacity and stiffness but has a significant impact on the ductility of the frame.

1. Introduction

One of the most common lateral-load bearing systems is the reinforced concrete moment-resisting frame. In the cast-in-place method of constructing reinforced concrete frames, the construction joint or cold-joint occurs due to concreting interruption. In fact, in multi-story reinforced concrete frames, cold-joint is inevitable because it is impossible to perform the entire concreting operation at once. Principally, cold-joint must be located where it has the least interference with the performance of the structure. According to ACI 224.3R-95 code [1], the appropriate location for cold-joint is at the top and bottom of the column, at the column-ceiling and column-floor joint zones. So far, much research has been done on the beam-column joint [2-14].

* *Corresponding Author: Assistant Professor, Department of Civil Engineering, Bandargaz Branch, Islamic Azad University, Bandargaz, Iran. Email: Ehsan.Karimi@iau.ac.ir*

** *Associate Professor, Department of Civil Engineering, Shahrood University of Technology, Shahrood, Iran.*

https://doi.org/10.52547/NMCE.2022.365

Numerous studies have also been conducted on the performance of joints in precast concrete structures [15-21]. However, it should be noted that cold-joint in precast concrete structures, in both terms of details and location, is different from cast-in-place concrete structures. Therefore, not much research has been conducted on cold-joint located in the cast-in-place reinforced concrete moment-resisting frames, which was constructed practically according to the recommendation of ACI 224.3R-95. Roy and Laskar [22] carried out a study on the behavior of the beam-column joint with cold-joint located at the bottom of the beam. In another study, Roy and Laskar [23] investigated the behavior of a beam-column joint with cold-joint located at both the top and bottom of the beam. In the present study, initially, the modeling of a single-story single-span reinforced concrete frame has been performed monolithically. Besides, the modeling of cold-joint behavior has been done in both opening mode (Mode I) and sliding mode (Mode II) of fracture mechanics. Subsequently, cold-joint has been placed on the frame columns at the column-floor and

column-ceiling joint zones. Eventually, the behavior of the single-story reinforced concrete frame with cold-joint has been evaluated in comparison with the monolithic frame in three modes of one, two, and three spans under monotonic lateral load.

2. Numerical modeling

In this research, finite element software Abaqus (Abaqus 2017) has been employed for nonlinear numerical analysis of models. In order to increase accuracy, all physical elements in reinforced concrete, including concrete and steel reinforcement, are modelled separately. An 8-node linear hexahedral solid element with reduced integration (C3D8R) was used to model concrete, and a 2-node linear beam element (B31) was utilized to model steel bars. In order to model the behavior of concrete, the concrete damaged plasticity model (CDP) was used with the parameters presented in Table 1.

Table 1: Parameters of CPD**.**

ψ	ε	f_{bo}/f_{co}	K_c
36	0.1	1.16	0.667

Here, ψ is the dilatancy angle measured in the p-q deviatory plan at high confining pressure, ε is the eccentricity of plastic potential surface, f_{bo} and f_{co} are the biaxial and uniaxial compressive yield strengths, respectively, and k_c is the ratio between the magnitudes of deviatoric stress in uniaxial tension and compression [24]. The uniaxial compressive stress-strain behavior of concrete is considered based on the theoretical equations proposed by Desayi and Krishnan [25], which are presented as follows:

$$f = \frac{E_c \varepsilon}{1+\left(\frac{\varepsilon}{\varepsilon_0}\right)^2} \quad (1)$$

$$E_c = \frac{2f_c^{'}}{\varepsilon_0} \quad (2)$$

In these equations, f_c' is the compressive strength of the cylindrical concrete specimens, f, ε_0, and E_0 are respectively the stress at the assumed strain of ε, the strain corresponding to the concrete ultimate compressive strength, and the concrete modulus of elasticity. The value of ε_0 is obtained from the equation provided by Majewski [26], which is as follows:

$$\varepsilon_0 = 0.0014[2-\exp\left(-0.024f_c^{'}\right)-\exp\left(-0.140f_c^{'}\right)] \quad (3)$$

The uniaxial tensile stress-strain behavior of concrete is also considered based on the model proposed by Massicotte et al. [27], which is shown in Figure 1:

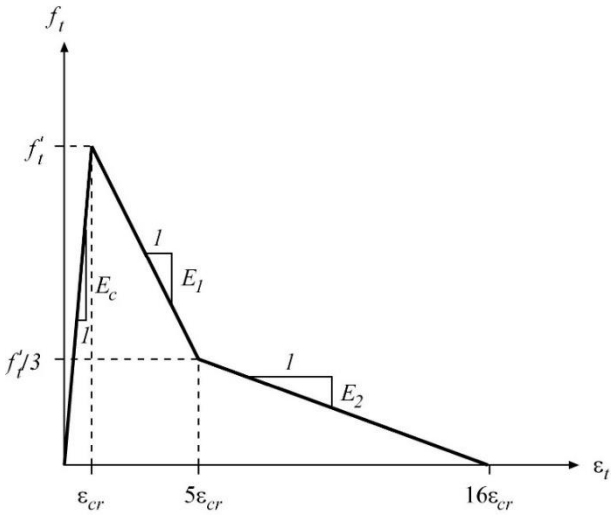

Fig. 1: Massicotte et al. [27] tension stiffening model.

In this model, f_c' and ε_{cr} are the maximum tensile strength and the strain corresponding to the maximum tensile strength, respectively. The maximum tensile strength is obtained from the equation provided in the FIB Model Code [28], which is as follows:

$$f_{ctm} = 0.3\left(f_{ck}\right)^{2/3} \quad (4)$$

Where f_{ctm} and f_{ck} are the average axial tensile strength and the characteristic compressive strength of concrete in Mpa, accordingly. One of the other parameters required for the CDP model is the damage parameter. Lubliner et al. [29] have proposed a simple damage model in which plastic degradation occurs only within the softening range, and the stiffness is proportional to the cohesion of the material:

$$d = 1-\frac{c}{c_{\max}} \quad (5)$$

where c is the cohesion in the yield criteria, which is proportional to the stress and c_{max} is proportional to the strength of the concrete. In the state of uniaxial tension or compressive, Equation 5 is simplified as follows [30]:

$$d = 1-\frac{f}{f_c^{'}} \quad (6)$$

According to Figure 2, the bilinear elastoplastic model is used to model the behavior of steel reinforcements. The slope of the branch related to the stiffening zone is assumed to be constant and equal to 0.01 of the gradient of the curve in the elastic part. Sliding between reinforcements and

concrete is not considered in the modeling, and the steel bars are modeled as embedded region constraint in the concrete.

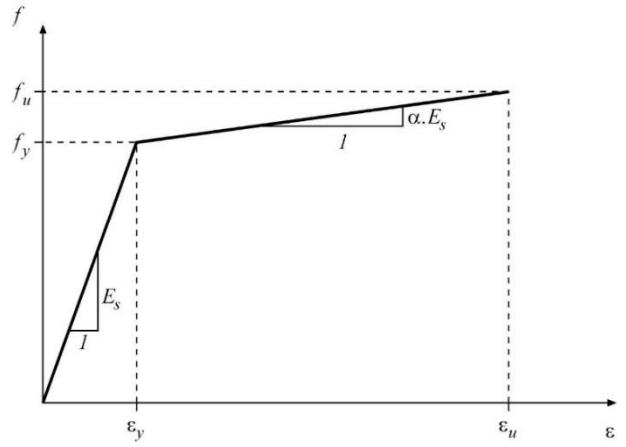

Fig. 2: Bilinear model for reinforcing steel behavior.

Here, f_y is yield stress, ε_y is strain corresponding to yield stress, f_u is ultimate stress, ε_u is strain corresponding to ultimate stress, E_s is the modulus of elasticity of steel, and α is the ratio of the slope of the curve in the stiffening part to the slope of the curve in the elastic part, which, in this study, is considered $\alpha = 0.01$.

In order to conduct this research, the results of some experimental studies have been used including, Al-Chaar et al. [31] study on reinforced concrete moment-resisting frame, Shah and Kishen [32] study on a three-point bending notched beam with cold-joint, and Júlio et al. [33] study on the push-off specimen with cold-joint.

2.1 Modeling of monolithic reinforced concrete frame

The model of Al-Chaar et al. [31] is used for numerical modeling of the monolithic reinforced concrete frame.

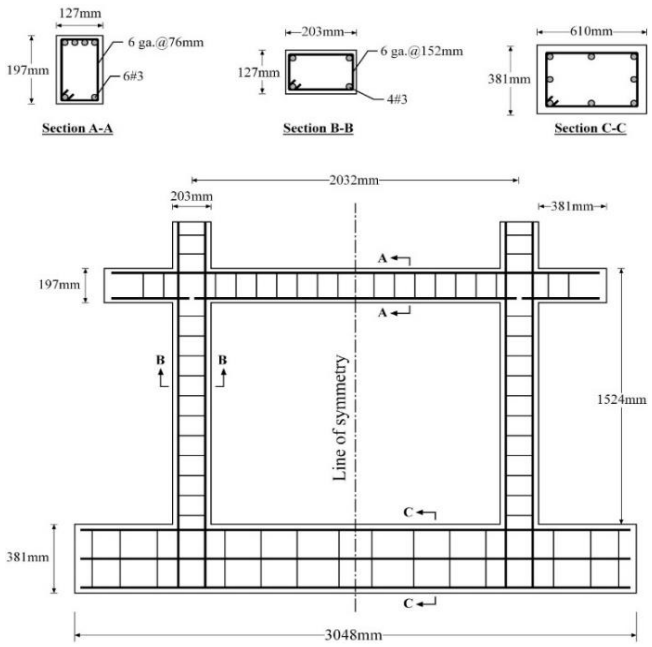

Fig. 3: Reinforcing and sections details of frame model.

The details of the single-story half-scale model of the reinforced concrete moment-resisting frame subjected to lateral in-plane monotonic loading tested by Al-Chaar et al. [31] are shown in Figure 3. The average compressive strength (f_c') and modulus of elasticity (E_c) of concrete were 38.438 MPa and 29992 Mpa, respectively, and the yield strength (f_y) and modulus of elasticity (E_s) of steel reinforcements were 338.5 Mpa and 200000 Mpa, accordingly. Figure 4 and Figure 5 display plots of compressive/tensile damage variable vs. crushing/cracking strain, respectively. The three-dimensional numerical model of the frame is shown in Figure 6.

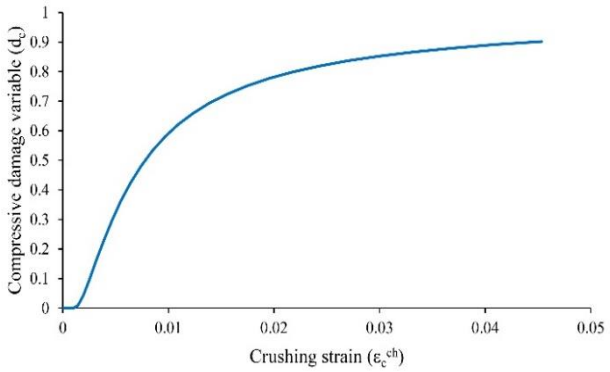

Fig. 4: Compressive damage variable vs. crushing strain.

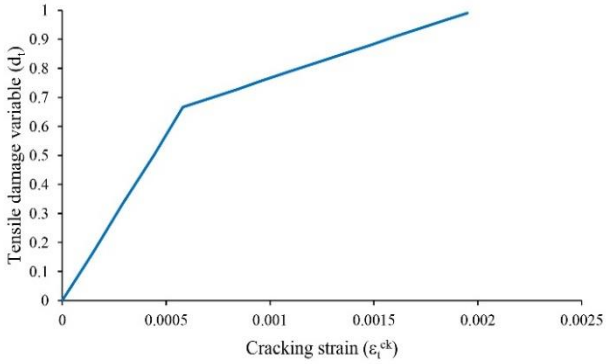

Fig. 5: Tensile damage variable vs. cracking strain.

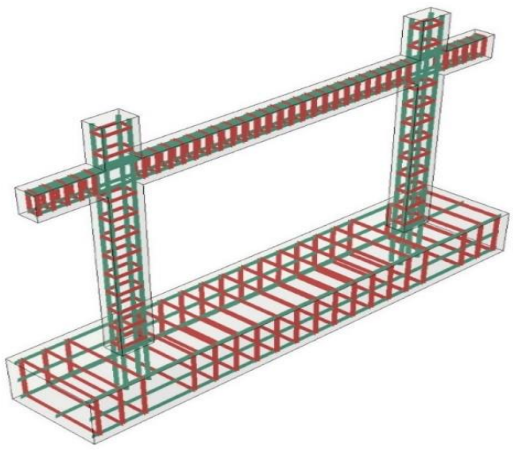

Fig. 6: 3D model of reinforced concrete frame.

The load is applied through a rigid plate attached to the free end of the beam. In view of the fact that in the experimental specimen, to eliminate any shear effect caused by friction between the force application device and the loading point on the specimen, greased plastic plates are placed in the numerical sample, the mentioned contact surfaces are also modeled without friction. The sample is laterally braced to eliminate out-of-plane movements. Moreover, considering the frame of Al-Chaar et al. [31] to be a nonductile frame, by modifying the reinforcement according to ACI 318-14 code [34] for medium ductility, this frame has also been studied for the ductile state according to Figure 7.

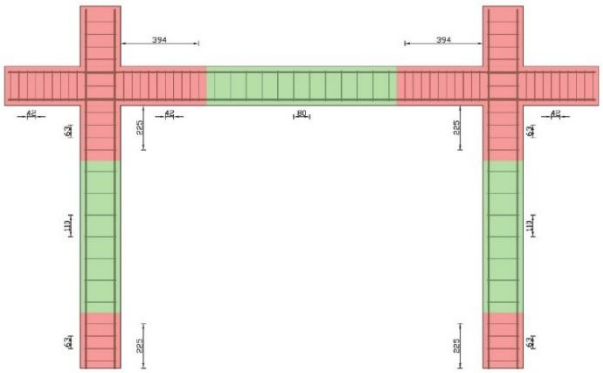

Fig. 7: Frame with modified reinforcement.

2.2 Modeling of mode I fracture (opening mode)

The model of Shah and Kishen [32] has been used for numerical modeling of mode I fracture. Properties of geometrically similar notched beam specimens with different sizes with a transverse cold-joint in the middle of the span under three-point bending with a span-to-depth ratio of 2.5 (S/b), a notch-to-depth ratio of 0.2 (a_0/b) and a notch width of 2mm tested by Shah and Kishen [32] are shown in Figure 8 and Table 2. The average compressive strength on both sides of the cold-joint is the same and equal to 34 MPa.

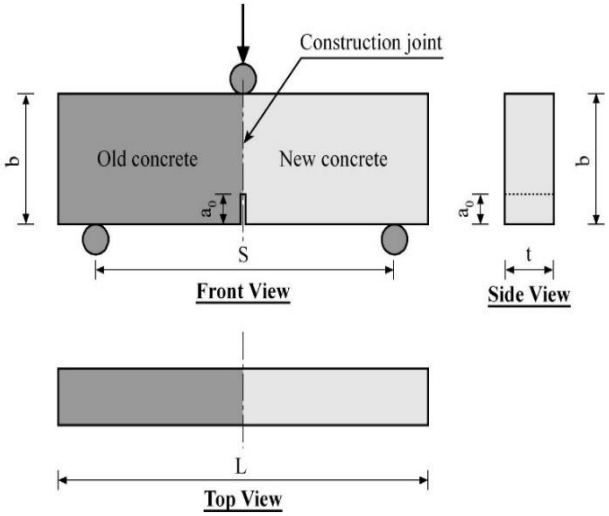

Fig. 8: Details of the three-point bending beam specimens.

Table 2: Dimensions of beams (mm).

Beam dimension	Small	Medium	Large
Depth(b)	76	152	304
Length(L)	241	431	810
Span(S)	190	380	760
Thickness(t)	50	50	50
Notch size(a_0)	15.2	30.4	60.8

The three-dimensional model of the modeled beams is shown in Figure 9.

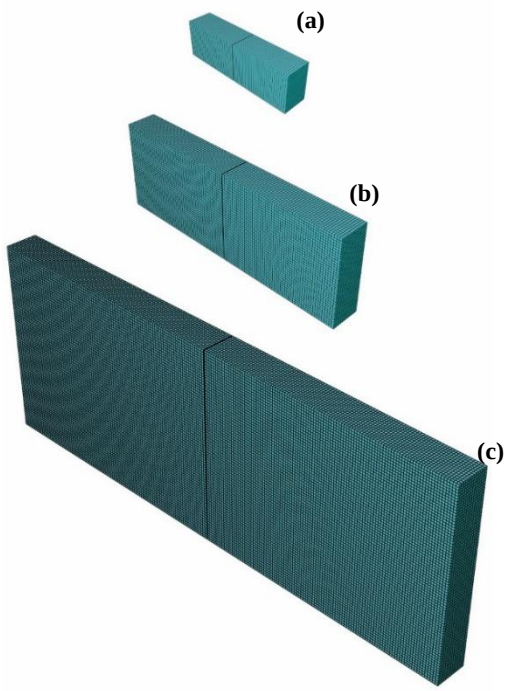

Fig. 9: 3D model of beam in: (**a**) small, (**b**) medium, and (**c**) large size.

Instead of defining a new element, such as the cohesive element, to model the cold-joint, the capability of surface-based cohesive behavior has been used because of the small thickness of the cold-joint [35]. In this case, the mechanical properties of the surface are assigned directly to the concrete contact surface. Equation 4 has been used to calculate the tensile strength. Moreover, to obtain the shear strength of concrete-to-concrete contact surface, for the unreinforced joint (τ_{Rdt}) in MPa and the fracture energy (G_f) in N/m, the equations provided in the FIB Model Code [28] are used, which are respectively presented as follows:

$$\tau_{Rdi} = c_a \cdot f_{ctd} + \mu \cdot \sigma_n \tag{7}$$

$$G_f = 73 \cdot f_{cm}^{0.18} \tag{8}$$

In these equations, c_a is a coefficient for the adhesive bond, and μ is the friction coefficient between two concrete surfaces in contact with each other, which are considered to be 0.2 and 0.6, respectively. σ_n is compressive stress resulting from an eventual normal force acting on the interface. f_{ctd} and f_{cm} are the tensile strength of concrete and the average compressive strength of concrete in Mpa, respectively.

Other required parameters of the mechanics of material are considered based on the theoretical equations proposed by Gere and Timoshenko [36]. Besides, according to the research of Gerges and Issa [37, 38], the tensile strength of concrete with cold-joint, and according to the study of Shah and Kishen [39], the fracture energy, can be reduced accordingly by 55% and 33% on average, compared to monolithic concrete.

2.3 Modeling of mode II fracture (sliding mode)

The model of Júlio et al. [33] has been used for numerical modeling of mode II fracture. The geometric details of the push-off specimens with cold-joint in three modes of having 2, 4, and 6 steel connectors tested by Júlio et al. [33], are shown in Figures 10 and 11, respectively. These samples have general dimensions of 254×546×127 mm3.

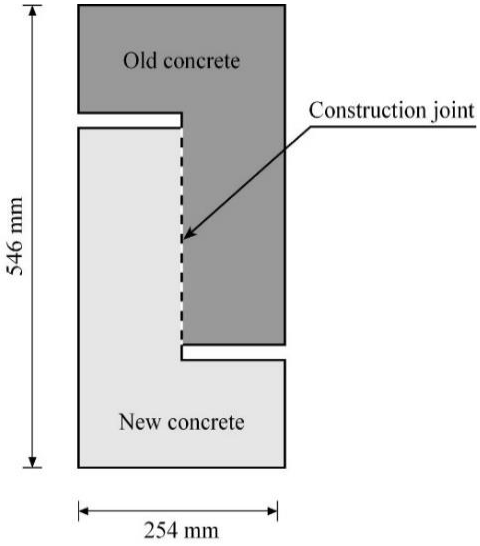

Fig. 10: Dimensions of push-off test specimens.

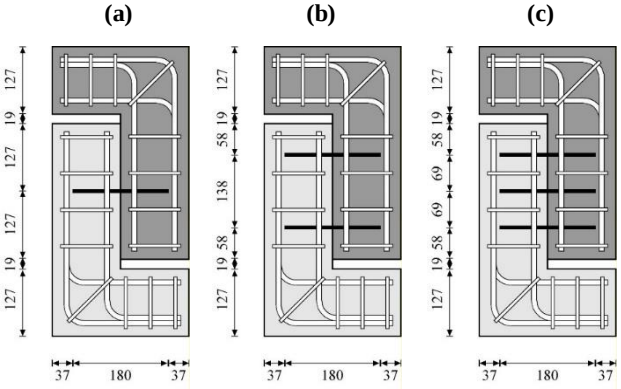

Fig. 11: The adopted push-off specimen (dimensions in mm) with: (**a**) two; (**b**) four; and (**c**) six steel connectors.

Each L-shaped half is reinforced with nine S400 steel bars with a diameter of 10mm and eight S400 steel stirrups with a diameter of 6mm. For steel connectors crossing the joint, S400 steel bars with a diameter of 6mm with an average yield strength of 433 MPa and a tensile strength of 533 MPa have been used. The average compressive strength of 28-day concrete is 43 MPa. The three-dimensional model of the modeled push-off specimen is shown in Figure 12.

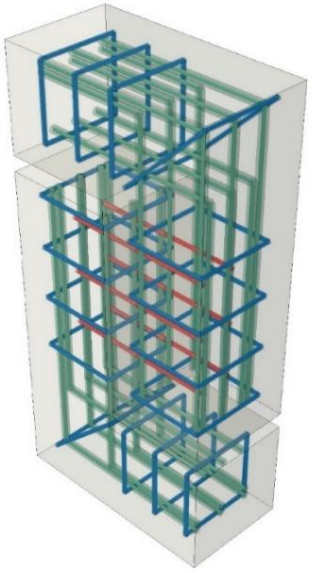

Fig. 12: 3D model of push-off specimen.

The boundary conditions of the push-off specimen subjected to monotonic loading are shown in Figure 13.

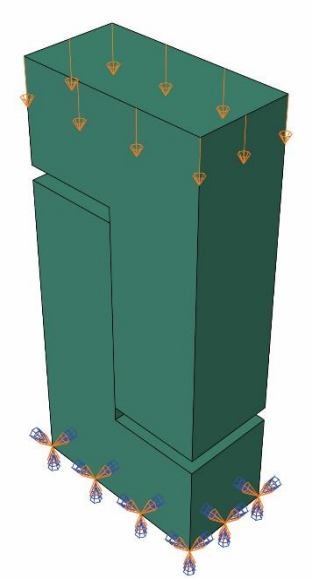

Fig. 13: Boundary conditions of push-off specimen.

All the details of modeling concrete, steel, and cold joint are analogous to the procedure used in modeling the frame and three-point bending beam described in the earlier sections.

2.4 Modeling of the reinforced concrete frame with cold-joint

Now, by modeling the cold-joint at the top and bottom of the columns at the column-floor and column-ceiling joint zones, according to Figure 14, the behavior of the frame with cold-joint in the previously modeled reinforced concrete moment-resisting frame can be investigated.

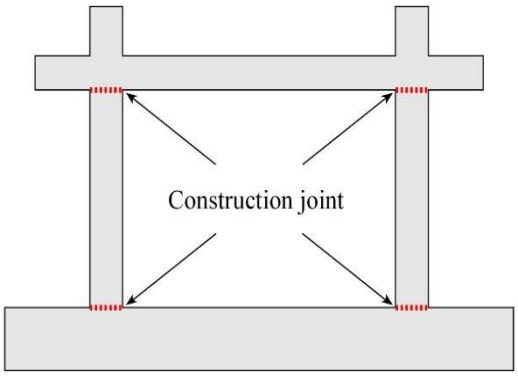

Fig. 14: Locations of cold-joints on the modeled frame**.**

2.5 Mesh Sensitivity Analysis

Mesh sensitivity analysis was performed to obtain the optimum element size in this numerical investigation. Four different mesh sizes were developed and analyzed. A uniform mesh size of 20, 35, and 50 mm are chosen for the concrete elements over the whole geometry in the frame and mesh size of 20 and 50 mm are chosen for concrete elements over connection areas and other areas in the frame, respectively, as shown in Figure 15. The same size for reinforcement mesh is also adopted for steel bars. Figure 16 shows a comparison between the different size meshes. Based on the results shown in Figure 16, a mesh size of 20mm for connection areas and 50 mm for other areas in the frame was adopted for the rest of the analysis.

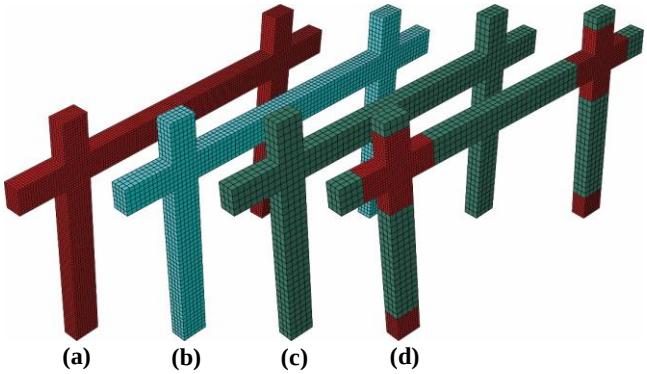

Fig. 15: Four different mesh sizes: (**a**) 20 mm; (**b**) 35 mm; (**c**) 50 mm; (**d**) 20 mm & 50 mm.

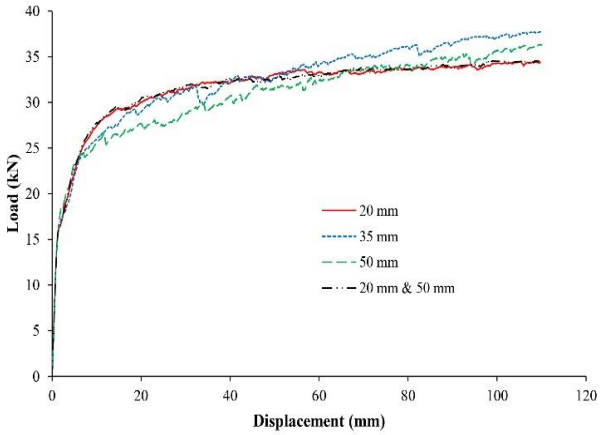

Fig. 16: Comparison between the different size meshes**.**

3. Verification

In the previous sections, numerical modeling of experimental specimens of the reinforced concrete moment-resisting frame of Al-Chaar et al. [31], the three-point bending notched beam with cold-joint of Shah and Kishen [32], and the push-off specimen with cold-joint of Júlio et al. [33] were presented. Figure 17 shows the load-displacement curve obtained from the numerical analysis of the reinforced concrete moment-resisting frame in both nonductile and ductile states together with the laboratory sample of Al-Chaar et al. [31], which reveals a good agreement between the numerical and experimental results. As can be seen, the modification of the frame reinforcement did not have any significant effect on the result of its numerical analysis, which was predictable due to the loading (monotonic load).

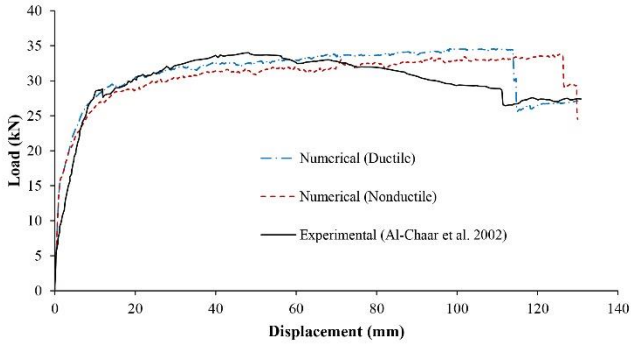

Fig. 17: Load versus Displacement curves.

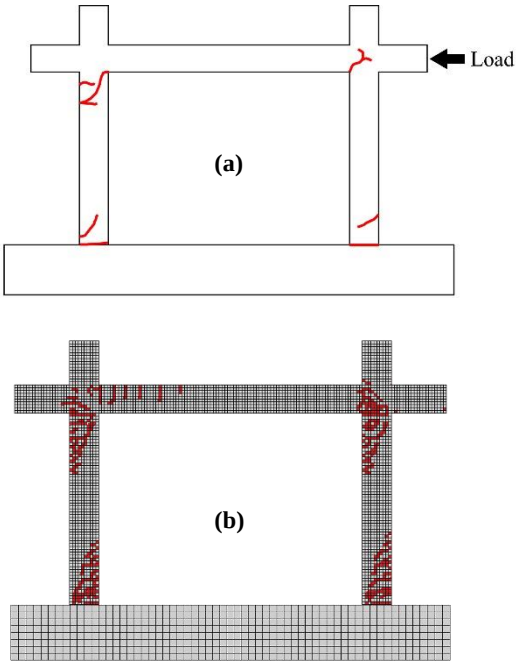

Fig. 18: Crack pattern for both (**a**) experimental [31] and (**b**)numerical.

In the numerical model as in the experimental model, cracks began to form in the beam–column joint on the tension side at approximately 1/10 of the total displacement. Next, in both models, a small tension crack appeared at the top of the compression column, shortly followed by both a tension crack near the base of the tension column and a shear crack near the base of the compression column. The residual strength of the experimental model and the numerical model stabilized at approximately 34.24 kN and 33.77 kN, respectively, after the formation of a plastic hinge. The crack pattern of the numerical and experimental models at the end of testing is shown in Figure 18.

Figure 19 displays the crack mouth opening displacement (CMOD) diagrams obtained from numerical analysis of the three-point bending beam with small, medium, and large sizes compared to Shah and Kishen's experimental diagrams [32], which shows a good agreement between the numerical and experimental results.

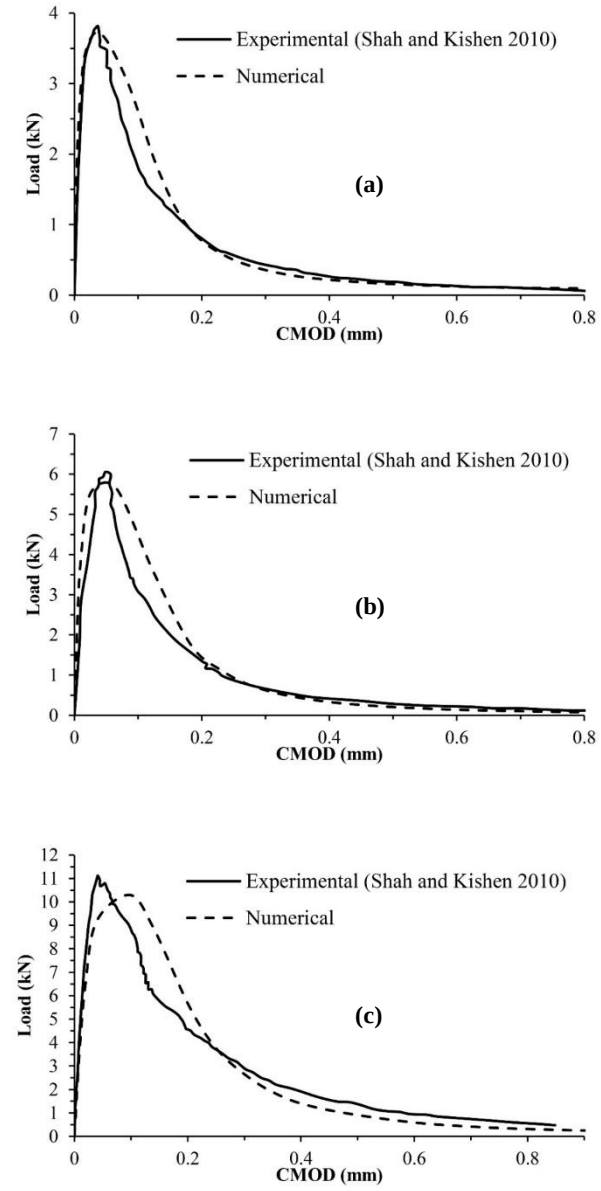

Fig. 19: Load versus CMOD curves for (**a**) small, (**b**) medium and (**c**) large beams.

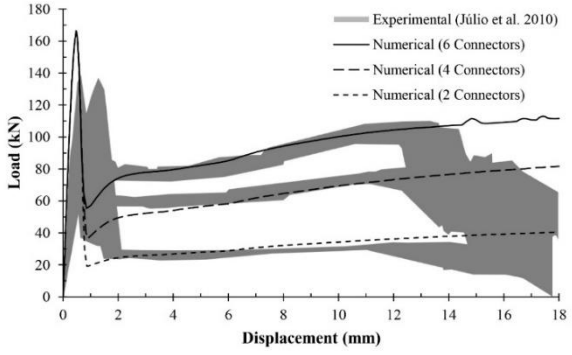

Fig. 20: Comparison of analytical and experimental load-displacement curves for push-off specimen with two, four and six steel connectors.

Figure 20 shows the load-displacement curves obtained from the numerical analysis of the push-off sample with three states of having 2, 4, and 6 steel connectors compared to the experimental samples of Júlio et al. [33], which indicates a good agreement between the numerical and experimental results.

4. Seismic performance parameters of the frame

The seismic performance of a system may be judged by specific parameters such as ultimate lateral capacity, stiffness, and ductility. Therefore, in this study, three parameters of ultimate lateral capacity, stiffness, and ductility have been used to investigate the effect of cold - joint on the single-story reinforced concrete moment-resisting frame with one, two, and three spans. All three of these parameters can be obtained from the idealized bilinear load-displacement curve. So far, different methods have been proposed to plot the idealized bilinear load-displacement curve [40-45].

In this study, the proposed method of Paulay and Priestley [41], shown in Figure 21, has been employed. To define the yield displacement (δ_y), a line can be drawn on the force-displacement envelope curve between the point of origin and the point corresponding to the first yield of the longitudinal reinforcements, or 75% of the ultimate force P_u (whichever is less), and extended up to the level of P_u. The amount of displacement corresponding to a 20% drop in maximum load or buckling of longitudinal reinforcement or fracture of longitudinal or transverse reinforcement (whichever occurs sooner) can also be defined as the ultimate displacement (δ_u) [40].

Eventually, the branch after yielding can be drawn on the idealized bilinear load-displacement curve using an iterative graphical procedure so that the areas below and above the ideal two-line curve become equal, as shown in Figure 21.

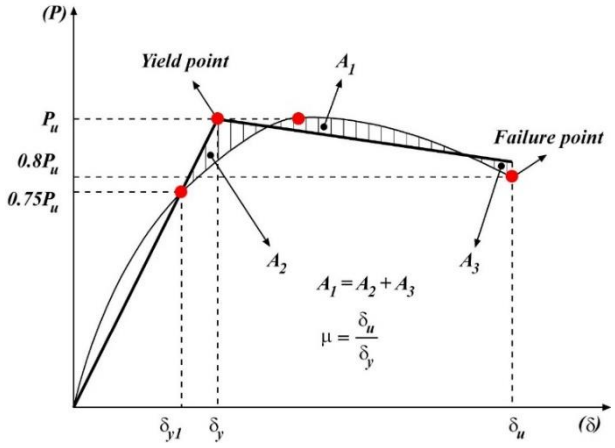

Fig. 21: Method used to draw ideal bilinear force–displacement curve.

Here the ultimate force P_u is the ultimate lateral capacity of the frame. The slope of the first branch of the idealized bilinear curve is defined as the stiffness, and the ratio of the ultimate displacement (δ_u) to the yield displacement (δ_y) is defined as ductility, according to the following equation:

$$\mu = \frac{\delta_u}{\delta_y} \tag{9}$$

Figure 22 shows the load-displacement curve obtained from the numerical analysis of the monolithic frame compared to the frame with cold-joint in three states of one, two, and three spans. Figure 23 also shows the idealized bilinear curve related to the single-story single-span monolithic frame and the frame with cold-joint.

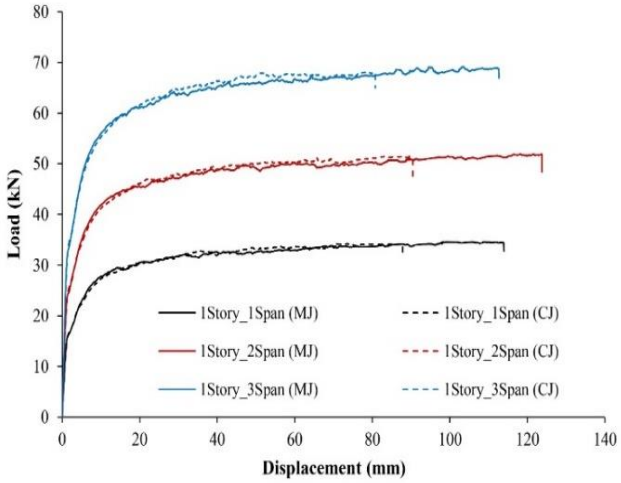

Fig. 22: load-displacement curve obtained from the numerical analysis of the monolithic frame, compared to the frame with cold-joint in three states of one, two, and three spans.

Table 3: Values of parameters used for frame modeling.

concrete parameters	value	Steel parameters	value
$f_c'\ (MPa)$	38.438	$f_y\ (MPa)$	338.5
$f_t'\ (MPa)$	3.416	$f_u\ (MPa)$	545.0
$E_c\ (MPa)$	29,992	$E_s\ (MPa)$	200,000
$\varepsilon_0\ (m/m)$	0.00256	$\varepsilon_y\ (m/m)$	0.00169
$\varepsilon_{cr}\ (m/m)$	0.00011	$\varepsilon_u\ (m/m)$	0.096

The values of parameters used for frames modeling are tabulated in Table 3.

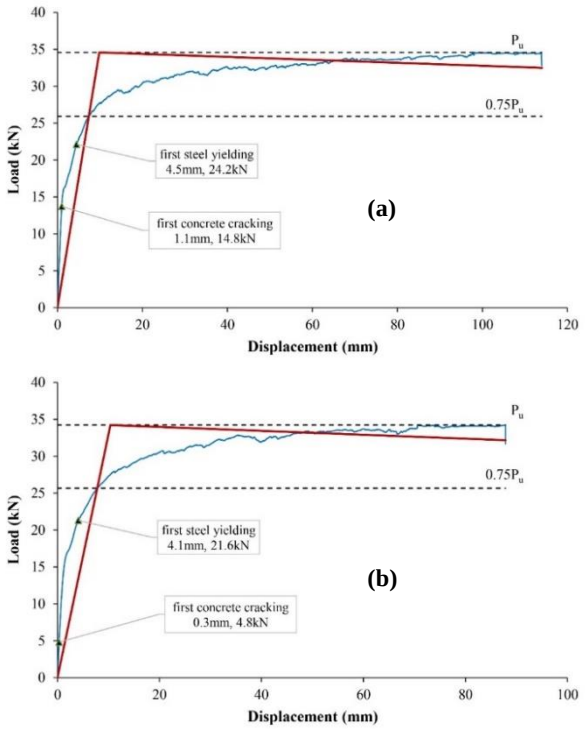

Fig. 23: Idealized bilinear curve related to the single-story single-span (**a**) monolithic frame and (**b**) the frame with cold-joint.

The first crack in concrete, first yield of reinforcement, and tensile damage variable of monolithic frame and frame with cold-joint are shown in Figures 24 to 31 for the one span. Figure 32 shows the status of cold-joints at ultimate displacement for the single-span frame with cold-joint.

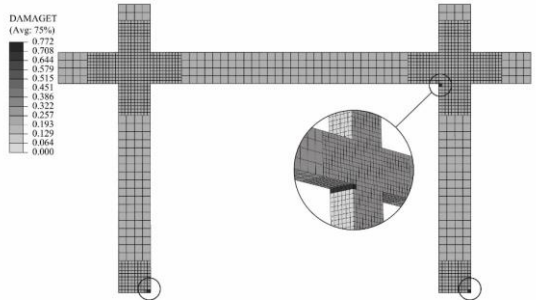

Fig. 24: First crack in concrete at force 14.8 kN and displacement 1.1 mm for the single-span monolithic frame.

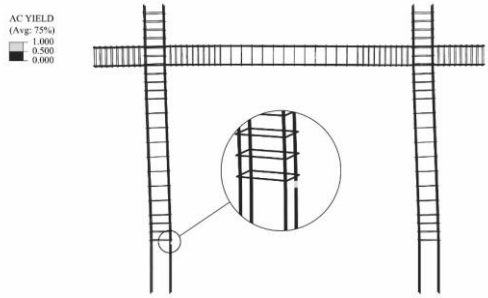

Fig. 25: First yield of reinforcement at force 24.2 kN and displacement 4.5 mm for the single-span monolithic frame.

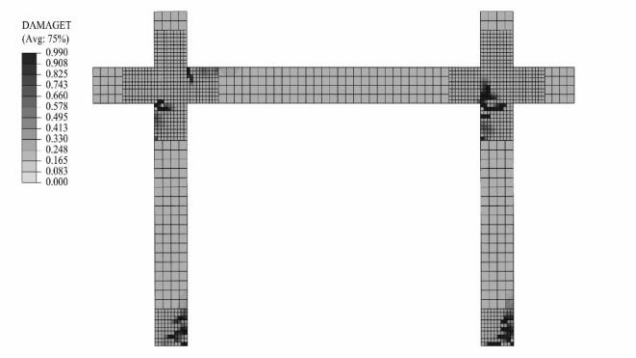

Fig. 26: Tensile damage variable at the moment of the first yield of reinforcement for the single-span monolithic frame.

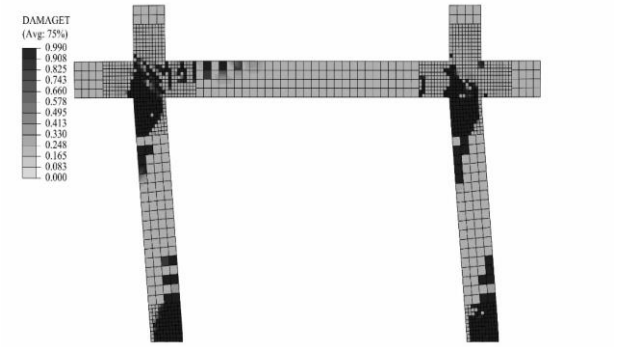

Fig. 27: Tensile damage variable at ultimate displacement for the single-span monolithic frame.

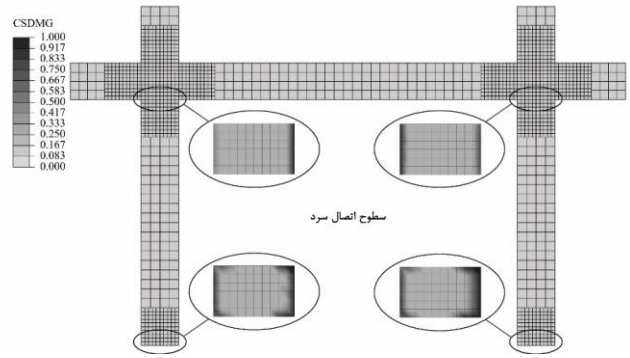

Fig. 28: First crack in concrete at force 4.8 kN and displacement 0.3 mm for the single-span frame with cold-joint.

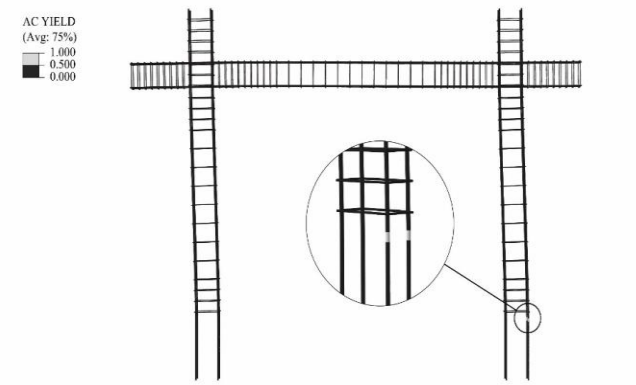

Fig. 29: First yield of reinforcement at force 21.6 kN and displacement 4.1 mm for the single-span frame with cold-joint.

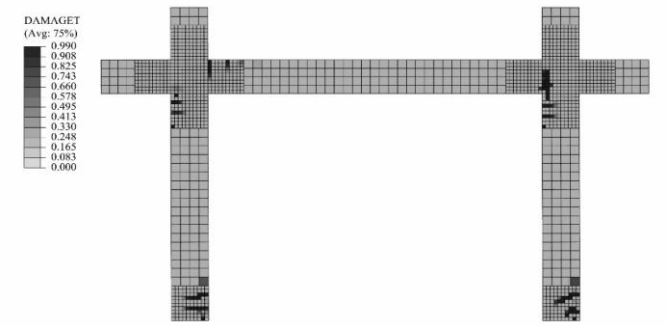

Fig. 30: Tensile damage variable at the moment of the first yield of reinforcement for the single-span frame with cold-joint.

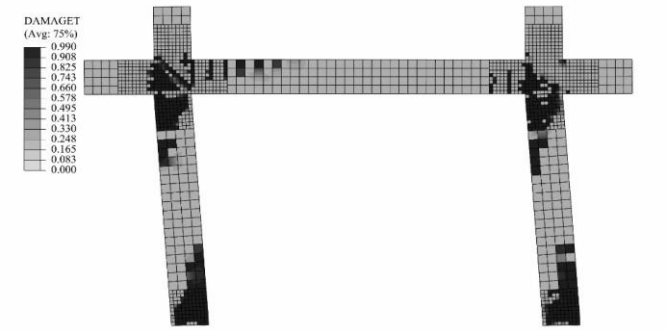

Fig. 31: Tensile damage variable at ultimate displacement for the single-span frame with cold-joint.

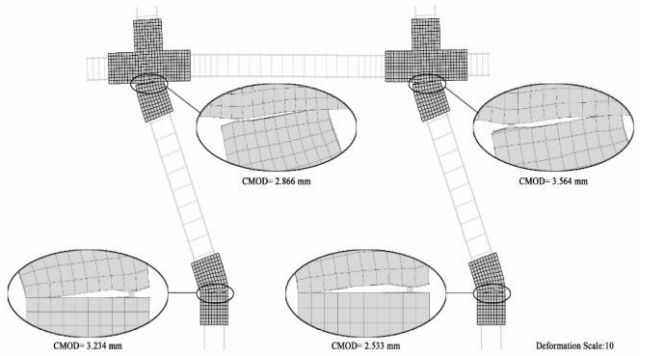

Fig. 32: Cold-joint status at ultimate displacement for the single-span frame with cold-joint.

The three-dimensional model of the single-story frame with one, two, and three spans is shown in Figure 33.

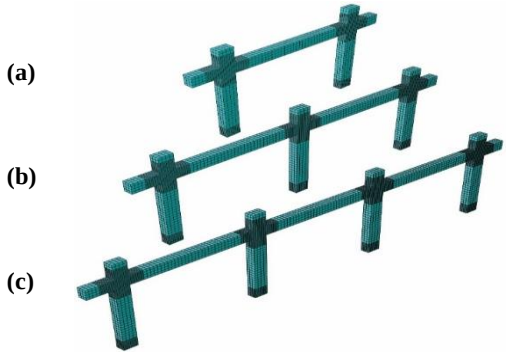

Fig. 33: 3D model of the single-story frame with: (**a**) one, (**b**) two, and (**c**) three spans.

The values of yield displacement, displacement corresponding to the first crack, displacement corresponding to the first yield of reinforcement, ultimate displacement, force corresponding to the first crack, force corresponding to the first yield, ultimate lateral capacity, stiffness, and ductility obtained for the monolithic frame and frame with cold-joint is presented in Table 4.

Table 4: The seismic performance of frames**.**

Parameter	One-span		Two-span		Three-span	
	MJ	**CJ**	**MJ**	**CJ**	**MJ**	**CJ**
Yield displacement δ_y (mm)	9.8	10.4	9.4	10.0	8.8	9.2
Displacement corresponding to the first crack (mm)	1.1	0.3	0.9	0.3	0.9	0.3
Displacement corresponding to the first yield of reinforcement (mm)	4.5	4.1	3.9	3.5	4.1	3.5
Ultimate displacement δ_u (mm)	114.0	87.9	123.8	90.5	112.7	80.8
Force corresponding to the first crack (kN)	14.8	4.8	19.5	7.4	26.3	9.7
Force corresponding to the first yield (kN)	24.2	21.6	31.9	30.9	43.8	41.3
Ultimate lateral capacity P_u (kN)	34.6	34.2	51.9	51.5	69.2	68.1
Stiffness (kN/mm)	3.5	3.3	5.3	5.1	7.5	7.4
Ductility $\mu = \delta_u / \delta_y$	11.6	8.5	13.1	9.0	12.7	8.8

The amount of change in ductility, ultimate lateral capacity, and stiffness of frames with cold-joint compared to the corresponding monolithic frames are shown in Table 5 and Figures 34 to 39 for the one, two, and three spans.

Table 5: The amount of change ductility, ultimate lateral capacity, and stiffness.

Number of spans	Ductility ratio (CJ/MJ) (%)	Ultimate lateral capacity ratio (CJ/MJ) (%)	Stiffness ratio (CJ/MJ) (%)
1	73	99	94
2	69	99	96
3	69	98	99
Average	**70**	**99**	**96**

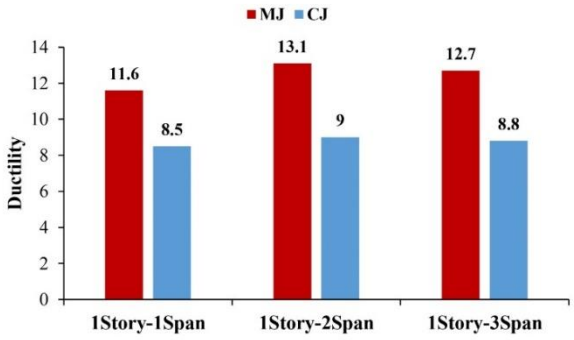

Fig. 34: Ductility of frames with cold-joint compared to the corresponding monolithic frames**.**

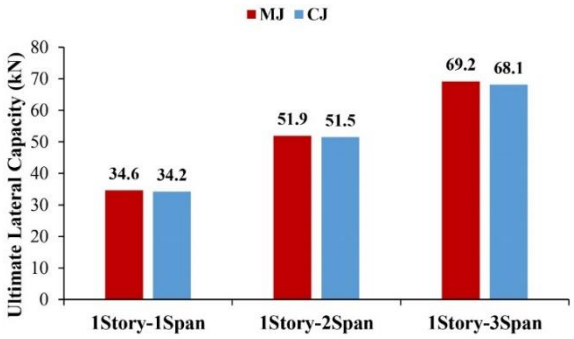

Fig. 35: Ultimate lateral capacity of frames with cold-joint compared to the corresponding monolithic frames.

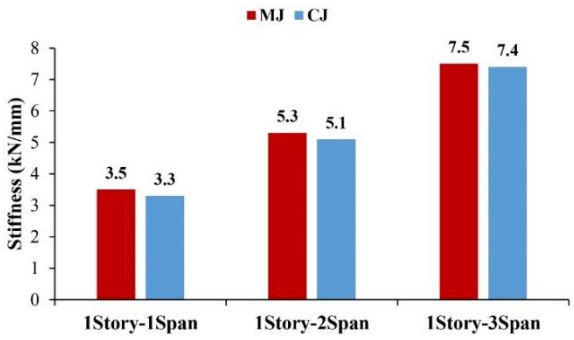

Fig. 36: Stiffness of frames with cold-joint compared to the corresponding monolithic frames.

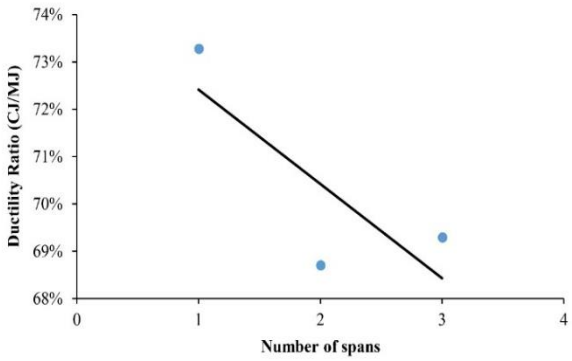

Fig. 37: The amount of change in ductility of frames with cold-joint compared to the corresponding monolithic frames.

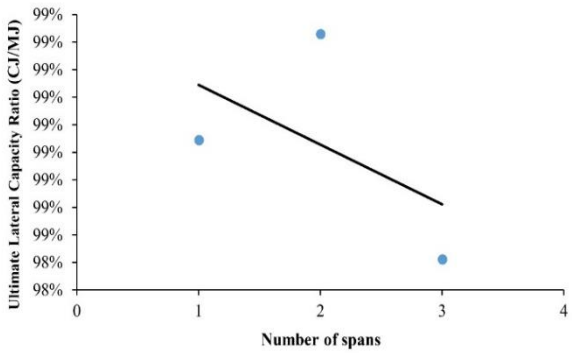

Fig. 38: The amount of change in ultimate lateral capacity of frames with cold-joint compared to the corresponding monolithic frames.

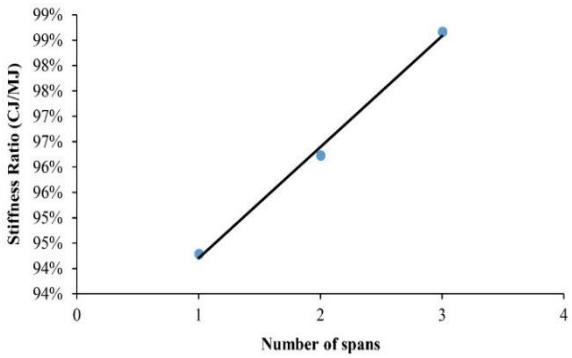

Fig. 39: The amount of change in stiffness of frames with cold-joint compared to the corresponding monolithic frames.

5. Conclusion

The results of the numerical study carried out in this research on the evaluation of the seismic performance parameters of reinforced concrete moment-resisting frame with cold-joint in comparison with the corresponding monolithic frame are summarized as follows:

1. The presence of cold-joint in the frame does not have a significant impact on its ultimate lateral capacity (the ultimate lateral capacity of the frame with cold-joint decreased by only about 1% compared to the monolithic frame).
2. The stiffness of the frame with cold-joint is reduced compared to the corresponding monolithic frame (about 4%)
3. The ductility of the frame with cold-joint is significantly reduced compared to the corresponding monolithic frame (about 30%).
4. The first crack in the frame with cold-joint occurs much faster than the corresponding monolithic frame (the first crack occurs in the frame with displacement and lateral strength of 70% and 64%, respectively; on average, less than that of the corresponding monolithic frame).
5. The first yield in steel bars occurs faster in the frame with cold-joint than the corresponding monolithic frame (The first yield in steel rebars occurs in the frame with cold-joint in displacement and lateral strength of 11% and 7%, respectively, relative to the corresponding monolithic frame).

Conflicts of interest

The authors declare that there is no conflict of interest.

References

[1] Halvorsen, G. T., Poston, R. W., Barlow, P., Fowler, D. W., Palmbaum, H. M., Barth, F. G., ... & Hansen, W. (2002). 224.3 R-95: Joints in Concrete Construction (Reapproved 2013). American Concrete Institute, ACI Committee, 224.

[2] Masi, A., Santarsiero, G., Lignola, G. P., & Verderame, G. M. (2013). Study of The Seismic Behavior of External RC Beam–Column Joints Through Experimental Tests and Numerical Simulations. Engineering Structures, 52, 207-219.

[3] Li, B., & Leong, C. L. (2015). Experimental and Numerical Investigations of The Seismic Behavior of High-Strength Concrete Beam-Column Joints With Column Axial Load. Journal of Structural Engineering, 141(9), e04014220.

[4] Barbhuiya, S., & Choudhury, A. M. (2015). A Study on The Size Effect of RC Beam–Column Connections Under Cyclic Loading. Engineering Structures, 95, 1-7.

[5] Somma, G., Pieretto, A., Rossetto, T., & Grant, D. N. (2015). RC Beam To Column Connection Failure Assessment and Limit State Design. Materials and Structures, 48(4), 1215-1231.

[6] Ning, N., Qu, W., & Ma, Z. J. (2016). Design Recommendations For Achieving "Strong Column-Weak Beam" In RC Frames. Engineering Structures, 126, 343-352.

[7] Mangalathu, S., & Jeon, J. S. (2018). Classification of Failure Mode and Prediction of Shear Strength For Reinforced Concrete Beam-Column Joints Using Machine Learning Techniques. Engineering Structures, 160, 85-94.

[8] Yang, H., Zhao, W., Zhu, Z., & Fu, J. (2018). Seismic Behavior Comparison of Reinforced Concrete Interior Beam-Column Joints Based on Different Loading Methods. Engineering Structures, 166, 31-45.

[9] Oinam, R.M., Kumar, P., & Sahoo, D.R. (2019). Cyclic Performance of Steel Fiber-Reinforced Concrete Exterior Beam-Column Joints. Earthquakes and Structures, 16(5), 533-546.

[10] Alaee, P., & Li, B. (2020). Analytical Investigations of Reinforced Concrete Beam–Column Joints Constructed Using High-Strength Materials. Journal of Earthquake Engineering, 24(5), 774-802.

[11] Park, S. H., Yoon, D., Kim, S., & Geem, Z. W. (2021). Deep Neural Network Applied to Joint Shear Strength for Exterior RC Beam-Column Joints Affected by Cyclic Loadings. In Structures ,Elsevier, 33, 1819-1832.

[12] Borujerdi, A.S., et al. (2021). Evaluation of Structural Performance For Beam-Column Joints With High-Strength Materials Under Cyclic Loading Using PIV Technique. Journal of Building Engineering, e103283.

[13] Tonidis, M., & Sharma, A. (2021). Numerical Investigations on The Influence of Transverse Beams and Slab on The Seismic Behavior of Substandard Beam-Column Joints. Engineering Structures, 247, e113123.

[14] Sachdeva, P., Roy, A. D., & Kwatra, N. (2021). Behaviour of Steel Fibers Reinforced Exterior Beam-Column Joint Using Headed Bars Under Reverse Cyclic Loading. In Structures, 33, 3929-3943.

[15] Vidjeapriya, R., & Jaya, K. P. (2012). Experimental Study on Two Simple Mechanical Precast Beam-Column Connections Under Reverse Cyclic Loading. Journal of Performance of Constructed Facilities, 27(4), 402-414.

[16] Shariatmadar, H., & ZAMANI, B. E. (2014). An Investigation of Seismic Response of Precast Concrete Beam to Column Connections: Experimental Study. Asian Journal of Civil Engineering-Building And Housing, 15.

[17] Parastesh, H., Hajirasouliha, I., & Ramezani, R. (2014). A New Ductile Moment-Resisting Connection For Precast Concrete Frames In Seismic Regions: An experimental investigation. Engineering Structures, 70, 144-157.

[18] Adibi, M., Talebkhah, R., & Yahyaabadi, A. (2019). Simulation of Cyclic Response of Precast Concrete Beam-Column Joints. Computers and Concrete, 24(3), 223-236.

[19] Yu, J., Zhang, W., Tang, Z., Guo, X., & Pospíšil, S. (2020). Seismic Behavior of Precast Concrete Beam-Column Joints With Steel Strand Inserts Under Cyclic Loading. Engineering Structures, 216, e110766.

[20] Tarabia, A. M., Etman, E. E., Allam, S. M., & Aboelhassan, M. G. (2021). Modeling of Precast Reinforced Concrete Beam-column Joints Under Cyclic Loading. Journal of Earthquake Engineering, 26(14), 7626-7655.

[21] Elsanadedy, H. M. (2021). New Moment-Resisting Beam-Column Joints to Increase Progressive Collapse Resistance of Precast Concrete Buildings. Journal of Building Engineering, 44, e102884.

[22] Roy, B., & Laskar, A. I. (2017). Cyclic Behavior of In-Situ Exterior Beam-Column Subassemblies With Cold Joint In Column. Engineering Structures, 132, 822-833.

[23] Roy, B., & Laskar, A. I. (2018). Beam–Column Subassemblies With Construction Joint In Columns Above and Below The Beam. Magazine of Concrete Research, 70(2), 71-83.

[24] Alfarah, B., López-Almansa, F., & Oller, S. (2017). New Methodology For Calculating Damage Variables Evolution in Plastic Damage Model for RC structures. Engineering Structures, 132, 70-86.

[25] Desayi, P., & Krishnan, S. (1964). Equation For The Stress-Strain Curve of Concrete. In Journal Proceedings, 61(3), 345-350.

[26] Majewski, S. (2003). The Mechanics of Structural Concrete In Terms of Elasto-Plasticity. Publishing House of Silesian University of Technology, Gliwice.

[27] Massicotte, B., Elwi, A. E., & MacGregor, J. G. (1990). Tension-Stiffening Model For Planar Reinforced Concrete Members. Journal of Structural Engineering, 116(11), 3039-3058.

[28] Beverly, P. (2010). fib Model Code For Concrete Structures. New York: Wiley.

[29] Lubliner, J., Oliver, J., Oller, S., & Oñate, E. (1989). A Plastic-Damage Model For Concrete. International Journal of Solids and Structures, 25(3), 299-326.

[30] Tao, Y., & Chen, J. F. (2015). Concrete Damage Plasticity Model For Modeling FRP-To-Concrete Bond Behavior. Journal of Composites For Construction, 19(1), e04014026.

[31] Al-Chaar, G., Issa, M., & Sweeney, S. (2002). Behavior of Masonry-Infilled Nonductile Reinforced Concrete Frames. Journal of Structural Engineering, 128(8), 1055-1063.

[32] Shah, S.G., & Kishen, J.C. (2010). Nonlinear Fracture Properties of Concrete–Concrete Interfaces. Mechanics of Materials, 42(10), 916-931.

[33] Júlio, E. N. B. S., Dias-da-Costa, D., Branco, F. A. B., & Alfaiate, J. M. V. (2010). Accuracy of Design Code Expressions For Estimating Longitudinal Shear Strength of Strengthening Concrete Overlays. Engineering Structures, 32(8), 2387-2393.

[34] ACI, A. (2014). Building Code Requirements for Structural Concrete (ACI 318-14): Commentary on Building Code Requirements for Structural Concrete (ACI 318r-14): An ACI Report.

[35] Hibbett., Karlsson., & Sorensen. (1998). ABAQUS/standard: User's Manual, Vol. 1.

[36] Gere, J. M., & Timoshenko, S. P. (1997). Mechanics of Materials. Boston : PWS Publishing Company.

[37] Gerges, N. N., Issa, C. A., & Fawaz, S. (2015). Effect of Construction Joints on The Splitting Tensile Strength of Concrete. Case Studies in Construction Materials, 3, 83-91.

[38] Issa, C. A., Gerges, N. N., & Fawaz, S. (2014). The Effect of Concrete Vertical Construction Joints on The Modulus of Rupture. Case Studies in Construction Materials, 1, 25-32.

[39] Shah, S. G., & Kishen, J. C. (2010). Fracture Behavior of Concrete–Concrete Interface Using Acoustic Emission Technique. Engineering Fracture Mechanics, 77(6), 908-924.

[40] Park, R. (1989). Evaluation of Ductility of Structures and Structural Assemblages From Laboratory Testing. Bulletin of the New Zealand Society for Earthquake Engineering, 22(3), 155-166.

[41] Paulay, T., & Priestley, M. N. (1992). Seismic Design of Reinforced Concrete and Masonry Buildings. New York: Wiley.

[42] American Society of Civil Engineering. (2007). Seismic Rehabilitation of Existing Buildings.

[43] Council, B. S. S. (2000). Prestandard and Commentary for The Seismic Rehabilitation of Buildings (FEMA-356).

[44] Hwang, S. K., & Yun, H. D. (2004). Effects of Transverse Reinforcement on Flexural Behaviour of High-Strength Concrete Columns. Engineering Structures, 26(1), 1-12.

[45] Priestley, M., & Park, R. (1987). Strength and Ductility of Concrete Bridge Columns Under Seismic Loading. Structural Journal, 84(1), 61-76.